

EvaDrive: Evolutionary Adversarial Policy Optimization for End-to-End Autonomous Driving

Siwen Jiao^{1,3*}, Kangan Qian^{2,3*}, Hao Ye^{3*†}, Yang Zhong³, Ziang Luo^{2,3}, Sicong Jiang⁶, Zilin Huang⁷, Yangyi Fang², Jinyu Miao², Zheng Fu², Yunlong Wang², Kun Jiang², Diange Yang^{2‡}, Rui Fan⁴, Baoyun Peng^{5‡}

¹National University of Singapore ²Tsinghua University ³Xiaomi EV
⁴Tongji University ⁵Advanced Institute of Big Data, Beijing
⁶McGill University ⁷University of Wisconsin–Madison
e1349765@u.nus.edu

Abstract

Autonomous driving faces significant challenges in achieving human-like iterative decision-making, which continuously generates, evaluates, and refines trajectory proposals. Current generation-evaluation frameworks isolate trajectory generation from quality assessment, preventing iterative refinement essential for planning, while reinforcement learning methods collapse multi-dimensional preferences into scalar rewards, obscuring critical trade-offs and yielding scalarization bias. To overcome these issues, we present EvaDrive, a novel multi-objective reinforcement learning framework that establishes genuine closed-loop co-evolution between trajectory generation and evaluation via adversarial optimization. EvaDrive frames trajectory planning as a multi-round adversarial game. In this game, a hierarchical generator continuously proposes candidate paths by combining autoregressive intent modeling for temporal causality with diffusion-based refinement for spatial flexibility. These proposals are then rigorously assessed by a trainable multi-objective critic that explicitly preserves diverse preference structures without collapsing them into a single scalarization bias. This adversarial interplay, guided by a Pareto frontier selection mechanism, enables iterative multi-round refinement, effectively escaping local optima while preserving trajectory diversity. Extensive experiments on NAVSIM and Bench2Drive benchmarks demonstrate SOTA performance, achieving 94.9 PDMS on NAVSIM v1 (surpassing DiffusionDrive by 6.8, DriveSuprim by 5.0, and TrajHF by 0.9) and 64.96 Driving Score on Bench2Drive. EvaDrive generates diverse driving styles via dynamic weighting without external preference data, introducing a closed-loop adversarial framework for human-like iterative decision-making, offering a novel scalarization-free trajectory optimization approach.

Introduction

Autonomous driving has made significant advances in recent years (Qian et al. 2025a). These advances enable cars to navigate increasingly complex environments. Despite substantial progress in components such as perception (Qian et al. 2024b, 2025c), prediction (Wang et al. 2022; Shi et al.

2024), and planning (Fu et al. 2025; Qian et al. 2024c), integrating these capabilities into holistic driving behavior remains challenge. Central to this integration challenge is vehicle trajectory planning, which is the process of generating feasible, safe, and efficient motion trajectories.

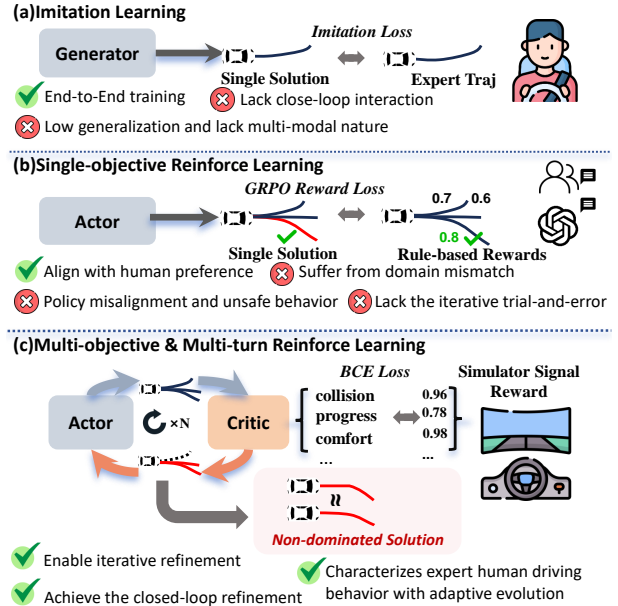


Figure 1: Comparison of end-to-end paradigms. (a) Imitation Learning: Mimics expert trajectories via imitation loss. (b) Single-objective Reinforcement Learning: Uses GRPO reward loss for preference alignment. (c) Proposed Multi-objective & Multi-turn Reinforcement Learning: Employs iterative Actor-Critic interaction for closed-loop refinement.

Traditional modular pipelines offer interpretability and decomposability, yet suffer from cumulative errors across stages. In contrast, end-to-end approaches (Hu et al. 2022, 2023) enable holistic optimization but often struggle with generalization and fail to model the inherent multimodality in complex driving decisions (Jiang et al. 2025b). Recently, generation-evaluation frameworks have

*Equal contribution.

†Project leader.

‡Corresponding author.

gained attention for their ability to reconcile diversity with controllability. Trajectory generators capture uncertainty by employing probabilistic models, such as diffusion-based approaches (Yu et al. 2024; Xing et al. 2025; Song et al. 2025) to synthesize diverse trajectory candidates. In parallel, evaluators learn differentiable scoring functions to rank these trajectories with respect to predefined multi-objective metrics (Chen et al. 2024a; Li et al. 2024b, 2025c).

Despite recent advances, current generation-evaluation frameworks treat planning and assessment as independent, sequential processes, lacking the closed-loop interaction essential to human-like decision-making. In contrast, expert drivers continuously generate, evaluate, and refine actions based on dynamic feedback. To bridge this gap, reinforcement learning (RL) methods have emerged as promising alternatives (Tang et al. 2025; Li et al. 2025b; Jiang et al. 2025a). Approaches like TrajHF (Li et al. 2025a) use GRPO to fine-tune trajectory models with human feedback, while DPO-style methods (Rafailov et al. 2023) optimize behavior via pairwise preference alignment. However, these methods face key limitations in autonomous driving. First, their reliance on human-annotated pairwise rankings introduces subjectivity and inconsistency, risking policy misalignment (Kiran et al. 2021). Second, their origins in language tasks lead to domain mismatch in continuous, high-dimensional driving settings (Zhou et al. 2025). Most critically, one-step optimization lacks the iterative refinement necessary for safe, adaptive planning—limiting robustness in safety-critical environments (Shani et al. 2024).

In fact, human drivers continuously evaluate and refine trajectory decisions through internal imagination and interaction with the environment, reasoning over multiple alternatives before committing to action. This observation motivates a key question: *Can autonomous driving cars leverage multi-modal trajectory proposals and multi-round refinement to enhance planning robustness and align with nuanced human preferences?* We answer affirmatively with **EvaDrive**, a novel framework that reformulates trajectory planning as a multi-objective reinforcement learning problem with genuine closed-loop interaction.

Unlike prior RL methods that collapse multi-dimensional preferences into scalar rewards, EvaDrive employs a trainable multi-objective reward model that preserves the structure of diverse preferences across safety, comfort, and efficiency without scalarization bias. Our approach is motivated by two key insights: autonomous driving provides naturally quantifiable metrics, avoiding noisy pairwise rankings required by GRPO; and feasible trajectories form a Pareto non-dominated set, where trade-offs across objectives exist. Traditional scalarization compresses these objectives into a single metric, obscuring optimal solutions and reducing policy diversity. EvaDrive uses adversarial co-evolution between a hierarchical generator and multi-objective critic to enable iterative multi-round refinement, escaping local optima while retaining RL’s trial-and-error nature. The main contributions are:

- **Hierarchical Planner:** Combines autoregressive intent modeling (to capture temporal causality) and diffusion-

based refinement (to provide spatial flexibility), enabling accurate trajectory modeling.

- **Multi-turn Optimization Mechanism:** Connects the trajectory generation and evaluation processes, achieving continuous adaptation through dynamic feedback, and skillfully avoids local optima by leveraging the Pareto frontier selection mechanism.
- **Adversarial Policy Optimization:** Through the dynamic game between the generator and evaluator, it not only drives continuous improvement of trajectory quality and effectively escapes local optima, but also enables the generation of trajectories with different styles by adjusting the dynamic weighting ratios of multiple optimization objectives.

Related Works

E2E AD

Imitation learning (IL) has been widely adopted for E2E trajectory planning in autonomous driving, where raw sensor inputs are mapped to expert demonstrations (Shao et al. 2023; Qian et al. 2024a, 2025b). UniAD (Hu et al. 2023), Transfuser (Chitta et al. 2022) leverage Bird-Eye-View (BEV) representations and introduce unified multi-task and safety-aware architectures to build planning-centric frameworks. VAD (Jiang et al. 2023) further improve this design by employing query-based representations and constructing a trajectory vocabulary, effectively transforming the problem from regression into a discrete classification task.

Recent benchmarks like NavSim (Dauner et al. 2024) advance E2E planning with multi-agent scenarios, while frameworks including Hydra-MDP (Li et al. 2024b), GTRS (Li et al. 2025c) and iPad (Guo et al. 2025) employ scorer-based trajectory synthesis integrating environmental interactions. However, these universally lack generator-scorer feedback loops. Contrastingly, our human decision-inspired solution integrates trajectory generation and evaluation within an iterative optimization cycle.

RL in generative task(multi-object and multi-turn)

RL has emerged as a critical paradigm for optimizing generative models in complex, goal-driven scenarios, particularly in multi-objective and multi-turn dialogue systems (Ouyang et al. 2022; Zhou et al. 2025; Shani et al. 2024). These tasks require balancing competing objectives (e.g., fluency, coherence, task success) and maintaining long-term context consistency across multiple interaction turns.

Key challenges include non-differentiable reward engineering, sparse-reward exploration-exploitation tradeoffs, and cross-user generalization. Emerging solutions integrate LLMs for reward modeling (Ouyang et al. 2022) and offline RL to reduce interaction costs (Gupta et al. 2023), while hybrid methods with pretrained dialogue systems (Yang, Li, and Quan 2021) balance task efficiency with natural fluency. In autonomous driving, post-training alignment methods like GRPO (Shao et al. 2024) and DPO (Rafailov et al. 2023) optimize human preference matching. Contrastingly, our framework pioneers multi-round multi-objective RL

with Adversarial Policy Optimization (APO) (Cheng et al. 2023) for trajectory optimization.

Problem Formulation

Reinforcement Learning for Autonomous Driving

Reinforcement Learning (RL) optimizes a policy $\pi_\theta(a | s)$ to maximize expected cumulative reward:

$$J(\theta) = \mathbb{E}_{s \sim \mathcal{D}, a \sim \pi_\theta} [R(s, a)], \quad (1)$$

where s and a denote state and action, respectively. In actor-critic frameworks, π_θ proposes actions (actor), and a reward function evaluates them (critic). For autonomous driving, π_θ plans future trajectories, with s encoding scene context and a representing the ego trajectory. The reward $\mathbf{R}_{\text{drive}}(s, a)$ reflects driving-specific objectives like safety, comfort, and traffic rule compliance.

Multi-Objective Optimization

Conventional RL approaches (e.g., DPO, GRPO) simplify complex decision-making to scalar reward maximization, insufficient for autonomous driving—which requires joint optimization of conflicting objectives: safety, comfort, efficiency, and rule adherence.

To capture this multi-faceted nature, we represent the driving reward as a **multi-objective vector**:

$$\mathbf{R}_{\text{drive}}(s, a) = [r_1(s, a), r_2(s, a), \dots, r_K(s, a)]^\top \in \mathbb{R}^K,$$

where each $r_i(s, a)$ corresponds to a distinct objective. The learning problem becomes maximizing the expected vector-valued return:

$$J(\theta) = \mathbb{E}_{(s,a) \sim \pi_\theta} [\mathbf{R}_{\text{drive}}(s, a)] \in \mathbb{R}^K. \quad (2)$$

For conflicting objectives (e.g., safety vs. efficiency), scalarization masks key trade-offs. Instead, we seek **Pareto-optimal solutions**—no other solution improves any objective without degrading at least one other—forming the target **Pareto frontier** for multi-objective optimization.

Reintroducing the Reward Model

To avoid limitations of implicit or oversimplified rewards, we adopt a reward learning approach akin to RLHF, introducing a learnable reward model r_ϕ that predicts $\mathbf{R}_{\text{drive}}(s, a)$, trained as follows:

- **Preference Data:** Ground-truth $\mathbf{R}_{\text{drive}}(s, a)$ derive from simulation-based trajectory metrics (e.g., obstacle proximity for safety, jerk for comfort).
- **Reward Model Training:** r_ϕ is supervised to match ground truth via MSE:

$$\phi^* = \arg \min_{\phi} \mathbb{E}_{(s,a) \sim \mathcal{D}} [\|r_\phi(s, a) - \mathbf{R}_{\text{drive}}(s, a)\|^2], \quad (3)$$

where $r_\phi(s, a) \in \mathbb{R}^K$ is the predicted reward vector.

- **Policy Optimization:** Trained r_ϕ serves as a differentiable proxy for environment feedback, enabling policy updates via multi-objective signals.

Method

Within the framework of multi-objective reinforcement learning, we now detail the core components of our approach, including the trajectory generation and evaluation modules (Actor and Critic), the multi-turn optimization mechanism, and the Adversarial Preference Optimization paradigm.

Trajectory Planner as Actor

We propose a lightweight structured trajectory planner, termed hierarchical modeling planner, serving as the **Actor** in our reinforcement learning framework. This Actor integrates two core components: an *autoregressive intent generator* and a *diffusion-based refiner*, aiming to address two critical challenges in planning: temporal causality modeling and refined optimization of global spatial trajectories under uncertainty. First, the current ego state \mathbf{s}_{ego} is extracted, based on which a Multi-Layer Perceptron (MLP) generates an initial set of candidate sequences $\mathbf{A}_0 \in \mathbb{R}^{N \times P \times 3}$ (where N denotes the number of sequences, P the number of poses per sequence, and 3 corresponds to xy -coordinates and yaw angle θ of each pose). Image features $\mathbf{F}_{\text{img}} \in \mathbb{R}^{H \times W \times D_f}$ (with $H \times W$ as spatial resolution and D_f as feature dimension) are extracted via a frozen visual backbone, serving as global environmental context.

Stage I: Autoregressive Intent Modeling The first stage models temporally coherent motion intent using a **Multi-Head Cross-Attention (MHCA)** mechanism, denoted as MHCA_T to emphasize its temporal specificity. Formally, the query vector \mathbf{Q} directly adopts the initial candidate sequences \mathbf{A}_0 ; the key vector \mathbf{K} and value vector \mathbf{V} are constructed by concatenating contextual features, all projected to a unified dimension via learnable linear transformations:

$$\mathbf{K} = \mathbf{V} = \text{concat}(\mathbf{A}_0, \mathbf{H}_{\text{hist}}, \mathbf{F}_{\text{img}}) \quad (4)$$

where $\mathbf{H}_{\text{hist}} \in \mathbb{R}^{M \times D_h}$ represents historical trajectory features (M as the number of historical timesteps, D_h as feature dimension). The temporal cross-attention operation is defined as:

$$\mathbf{A}_{\text{AR}} = \text{MHCA}_T(\mathbf{A}_0, \mathbf{K}, \mathbf{V}) \quad (5)$$

where $\mathbf{A}_{\text{AR}} \in \mathbb{R}^{T \times D_p}$ represents temporally optimized intent features as autoregressive candidates for refinement. A key design is the rectangular attention mask aligning \mathbf{Q} (of size T) with \mathbf{K} (of size $T + M + H \times W$), enforcing temporal causality by allowing each timestep in \mathbf{Q} to attend only to current and past elements in \mathbf{K} . This constraint is essential for learning time-dependent motion patterns (e.g., deceleration before turning) and preserving causal action order.

Stage II: Diffusion-Based Refinement Although the autoregressive module captures temporal coherence, it lacks capabilities in uncertainty modeling and spatial flexibility. To address this, forward noise is injected into \mathbf{A}_{AR} using the Denoising Diffusion Implicit Model (DDIM), generating stochastic inputs $\tilde{\mathbf{A}}^{(t)}$ at diffusion step t :

$$\tilde{\mathbf{A}}^{(t)} = \alpha_t \mathbf{A}_{\text{AR}} + \sigma_t \epsilon, \quad \epsilon \sim \mathcal{N}(0, \mathbf{I}), \quad \tilde{\mathbf{A}}^{(t)} \in \mathbb{R}^{N \times P \times 3} \quad (6)$$

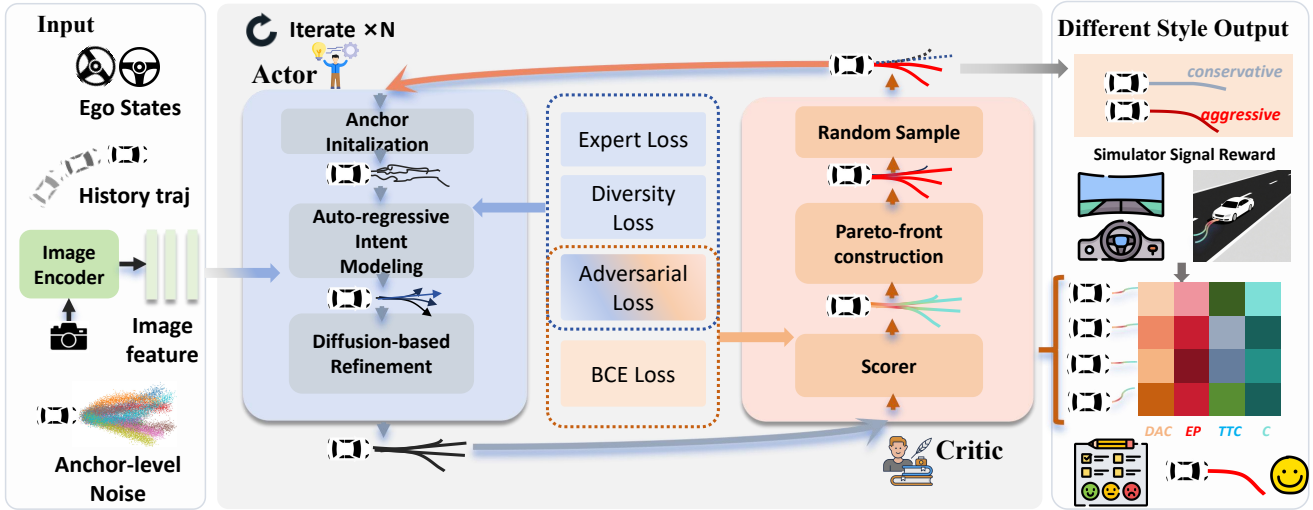


Figure 2: Overall framework of *EvaDrive*. Our method generates and evaluates trajectories in an end-to-end, multi-objective manner. (a) The Actor performs anchor initialization, intent modeling, and diffusion-based refinement to propose diverse trajectory candidates. (b) The Critic evaluates them using multi-objective simulator feedback and constructs a Pareto front. The best candidates are iteratively reused to guide future sampling, enabling style-adaptive and preference-aware planning.

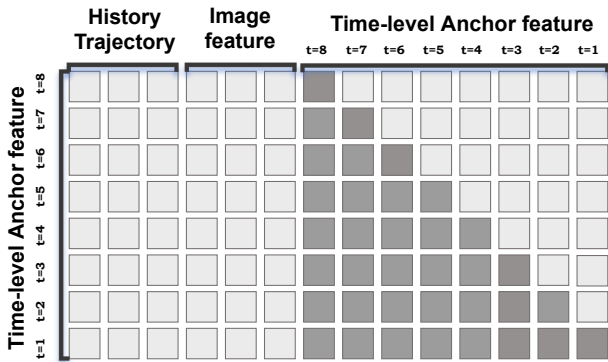


Figure 3: Attention Mask of Autoregressive Intent Generator, grey: visible elements, black: invisible elements

where α_t and σ_t are precomputed DDIM coefficients, and ϵ is a standard normal noise vector. These noisy candidates are refined via a second-stage module comprising spatial cross-attention MHCA_S followed by a lightweight Transformer decoder \mathcal{D}_θ . The spatial cross-attention operation is defined as:

$$\mathbf{A}_S = \text{MHCA}_S(\tilde{\mathbf{A}}^{(t)}, \mathbf{F}_{img}) \quad (7)$$

where $\mathbf{A}_S \in \mathbb{R}^{N \times P \times 3}$ denotes spatially augmented features. The decoder outputs denoised candidate features:

$$\hat{\mathbf{A}} = \mathcal{D}_\theta(\mathbf{A}_S), \quad \hat{\mathbf{A}} \in \mathbb{R}^{N \times P \times 3} \quad (8)$$

The final trajectory is decoded via an MLP:

$$\mathbf{T}_{\text{pred}} = \text{MLP}(\hat{\mathbf{A}}), \quad \mathbf{T}_{\text{pred}} \in \mathbb{R}^{N \times P \times 3} \quad (9)$$

Benefiting from the guidance of autoregressive features, our denoiser enables efficient trajectory generation through

single-step denoising, eliminating the need for multi-round inference in traditional diffusion models. This significantly improves computational efficiency, meeting the latency constraints of real-time deployment.

Reward Model as Critic

For reward-guided learning, we introduce a **reward model as critic** to evaluate predicted trajectories and provide multi-objective feedback for the planner. Unlike traditional scalar reward functions, it offers structured high-dimensional supervision, matching driving’s multi-objective nature.

Given the i -th predicted trajectory $\mathbf{T}_{\text{pred}}^{(i)}$, we first aggregate its temporal planning features (such as the denoised anchor features $\hat{\mathbf{A}}^{(i)}$ output by the second stage) via temporal max pooling:

$$\mathbf{v}^{(i)} = \text{MaxPool}_t(\hat{\mathbf{A}}^{(i)}), \quad \mathbf{v}^{(i)} \in \mathbb{R}^{D_p}. \quad (10)$$

The pooled $\mathbf{v}^{(i)}$ captures the global semantic intent of the trajectory, feeding a MLP that outputs N scalar reward components. The vector composed of these components from all trajectories collectively forms the driving reward vector $\mathbf{R}_{\text{drive}}^{(i)}$ defined earlier:

$$\mathbf{R}_{\text{drive}}^{(i)} = \text{MLP}(\mathbf{v}^{(i)}), \quad \mathbf{R}_{\text{drive}}^{(i)} \in \mathbb{R}^N. \quad (11)$$

Notably, trajectory evaluation is multi-objective: the critic estimates each objective independently (not as a single scalar), preserving reward diversity, avoiding premature aggregation, and enabling effective Pareto front exploration in subsequent optimization.

Multi-Turn Optimization Mechanism

Traditional single-step optimization in autonomous driving planning maximizes immediate rewards but lacks feedback

loops. While efficient, this unidirectional approach fails to support iterative refinement through trial-and-error, compromising reliability in safety-critical tasks despite a well-defined reward function $\mathbf{R}_{\text{drive}}$.

To address this, we propose a *multi-turn trajectory optimization mechanism* (Algorithm 1), which extends the existing multi-objective optimization framework into an iterative reinforcement-style process. Specifically, we define a total of K optimization rounds, indexed by $t = 0, 1, \dots, K - 1$. In each round, the actor policy π_θ generates a set of candidate trajectories conditioned on the current planning state s_t and, if applicable, guidance trajectories from the previous round. After completing all K rounds, we select the final output trajectory $a_{\text{final}} \in \mathcal{A}_{K-1}$ from the last candidate set.

We define the overall training objective by evaluating the final output trajectory using the multi-objective reward:

$$J_{\text{multi-turn}}(\theta) = \mathbb{E}_{\mathcal{M}, a_{\text{final}} \sim \pi_\theta} [\mathbf{R}_{\text{drive}}(s_{\text{final}}, a_{\text{final}})], \quad (12)$$

where s_{final} denotes the final planning state and a_{final} is selected from the candidate set \mathcal{A}_{K-1} . Here, $\mathbf{R}_{\text{drive}}$ denotes a task-level evaluation function that measures the overall quality of a completed trajectory in the final context.

During training, however, we require a more fine-grained and intermediate assessment of candidate trajectories at each round. To this end, we define a round-level multi-objective reward function $\mathbf{r}(\cdot)$, which shares the same dimensionality as $\mathbf{R}_{\text{drive}}$ but reflects local, per-round trajectory quality. This function acts as a vector-valued critic that outputs N scalar reward components per trajectory.

At each round t , the optimization process proceeds as follows:

First, the actor generates a set of candidate trajectories $\mathcal{A}_t = \{a_i\}$ based on the current planning context. For each trajectory $a \in \mathcal{A}_t$, the critic model evaluates its multi-dimensional reward vector:

$$\mathbf{r}(a) = [r^{(1)}(a), \dots, r^{(N)}(a)], \quad (13)$$

where N is the number of reward dimensions (e.g., safety, efficiency, comfort). The scalar functions $r^{(i)}(\cdot)$ represent the i -th reward component. Since these objectives often exhibit trade-offs, we avoid reward scalarization to preserve diversity in candidate behavior.

Instead, we extract the Pareto front \mathcal{P}_t from \mathcal{A}_t , defined as the set of all non-dominated trajectories:

$$\mathcal{P}_t = \{a_i \in \mathcal{A}_t \mid \nexists a_j \in \mathcal{A}_t, \mathbf{r}(a_j) \succ \mathbf{r}(a_i)\}, \quad (14)$$

where $\mathbf{r}(a_j) \succ \mathbf{r}(a_i)$ indicates that trajectory a_j dominates a_i , i.e., it performs at least as well in all reward dimensions and strictly better in at least one.

To promote exploration and mitigate overfitting to narrow solutions, we uniformly sample M guidance trajectories from the Pareto front:

$$\{\tilde{a}_t^{(m)}\}_{m=1}^M \sim \text{UniformSample}(\mathcal{P}_t), \quad (15)$$

which are used to condition the actor policy in the next round:

$$\mathcal{A}_{t+1} \leftarrow \pi_\theta(s_{t+1}, \{\tilde{a}_t^{(m)}\}_{m=1}^M). \quad (16)$$

Optionally, the planning state s_{t+1} can be updated based on the selected trajectory or a state transition function, enabling adaptive planning in dynamic environments. This mechanism enables principled multi-objective planning via Pareto-guided sampling and iterative policy refinement, supporting real-world autonomous driving.

Algorithm 1: Multi-Turn Trajectory Optimization

Input: Initial planning state s_0 , actor policy π_θ , reward function $\mathbf{r}(\cdot)$, total rounds K , sample size M

Output: Final output trajectory $a_{\text{final}} \in \mathcal{A}_{K-1}$

for $t = 0$ **to** $K-1$ **do**

1. Generate candidate trajectories

if $t = 0$ **then**

$\mathcal{A}_0 \leftarrow \pi_\theta(s_0)$;

else

$\mathcal{A}_t \leftarrow \pi_\theta(s_t, \{\tilde{a}_{t-1}^{(m)}\}_{m=1}^M)$;

2. Evaluate reward vectors for each trajectory

foreach $a \in \mathcal{A}_t$ **do**

$\mathbf{r}(a) = [r^{(1)}(a), \dots, r^{(N)}(a)]$;

3. Extract Pareto front from \mathcal{A}_t

$\mathcal{P}_t \leftarrow \{a_i \in \mathcal{A}_t \mid \nexists a_j \in \mathcal{A}_t, \mathbf{r}(a_j) \succ \mathbf{r}(a_i)\}$;

4. Sample guidance trajectories from \mathcal{P}_t

$\{\tilde{a}_t^{(m)}\}_{m=1}^M \sim \text{UniformSample}(\mathcal{P}_t)$;

5. Update planning state (if applicable)

$s_{t+1} \leftarrow \text{UpdateState}(s_t, a_t)$;

6. Select final output trajectory

$a_{\text{final}} \in \mathcal{A}_{K-1}$;

 // based on $\mathbf{R}_{\text{drive}}$ evaluation

return a_{final} ;

Adversarial Policy Optimization (APO)

To enable preference-aware trajectory optimization, we propose APO, a learning paradigm that frames policy training as a multi-objective optimization problem with adversarial reward learning. This approach draws inspiration from adversarial training principles while specifically addressing the multi-dimensional nature of autonomous driving evaluation tasks. Given a trajectory policy π_θ and a learnable multi-objective reward model r_ϕ that outputs a reward vector:

$$\mathbf{R}_{\text{drive}}(s, a) = [r_\phi^{(1)}(s, a), \dots, r_\phi^{(N)}(s, a)]^\top \in \mathbb{R}^N \quad (17)$$

where N denotes the number of distinct driving performance metrics (e.g., safety, comfort, efficiency), we define the core objective of APO. Let $\mathcal{D}_{\text{expert}} = \{(s_j, a_j)\}_{j=1}^M$ denote the expert demonstration dataset. For each objective dimension $i \in \{1, \dots, N\}$, we define:

$$V^{(i)}(\phi, \theta) = \mathbb{E}_{(s,a) \sim \pi_\theta} [r_\phi^{(i)}(s, a)] - \mathbb{E}_{(s,a) \sim \mathcal{D}_{\text{expert}}} [r_\phi^{(i)}(s, a)]. \quad (18)$$

The overall optimization is a vector-valued objective:

$$\min_{\phi} \max_{\theta} \mathbf{V}(\phi, \theta) = [V^{(1)}(\phi, \theta), \dots, V^{(N)}(\phi, \theta)]^\top. \quad (19)$$

Here, the policy generator (\max_{θ}) aims to produce trajectories that maximize the reward predictions across all dimensions, while the reward model (\min_{ϕ}) learns to assign higher rewards to expert demonstrations than to generated trajectories, providing gradients that guide the generator toward expert-like behavior.

Multi-Objective Optimization with Weighted Scalarization The optimization addresses a multi-objective problem where each reward component $r_{\phi}^{(i)}(s, a)$ corresponds to a distinct driving performance metric. To make the problem computationally tractable, we employ weighted scalarization (Zadeh 1963) using a preference vector $\mathbf{w} = \{w_i\}_{i=1}^N$ with $\sum_{i=1}^N w_i = 1$ and $w_i \geq 0$. The scalarized objective:

$$\min_{\phi} \max_{\theta} V_{\mathbf{w}}(\phi, \theta) = \sum_{i=1}^N w_i \cdot V^{(i)}(\phi, \theta). \quad (20)$$

Different choices of \mathbf{w} enable the generation of trajectories with distinct behavioral characteristics.

Generator Optimization ($\max_{\theta} V_{\mathbf{w}}$) The generator is updated using the policy gradient:

$$\nabla_{\theta} V_{\mathbf{w}}(\phi, \theta) = \sum_{i=1}^N w_i \cdot \mathbb{E}_{(s,a) \sim \pi_{\theta}} \left[\nabla_{\theta} \log \pi_{\theta}(a|s) \cdot r_{\phi}^{(i)}(s, a) \right], \quad (21)$$

with the parameter update:

$$\theta \leftarrow \theta + \eta_{\theta} \cdot \nabla_{\theta} V_{\mathbf{w}}(\phi, \theta). \quad (22)$$

This weighted approach converts the multi-objective optimization into a single-objective problem while enabling diverse trajectory styles via \mathbf{w} (Marler and Arora 2004).

Reward Model Optimization ($\min_{\phi} V_{\mathbf{w}}$) The reward model is trained to distinguish between generated and expert trajectories by minimizing:

$$\nabla_{\phi} V_{\mathbf{w}}(\phi, \theta) = \sum_{i=1}^N w_i \cdot \left[\mathbb{E}_{(s,a) \sim \pi_{\theta}} [\nabla_{\phi} r_{\phi}^{(i)}(s, a)] - \mathbb{E}_{(s,a) \sim \mathcal{D}_{\text{expert}}} [\nabla_{\phi} r_{\phi}^{(i)}(s, a)] \right], \quad (23)$$

with the parameter update:

$$\phi \leftarrow \phi - \eta_{\phi} \cdot \nabla_{\phi} V_{\mathbf{w}}(\phi, \theta). \quad (24)$$

This ensures the reward model maintains balanced discriminative capability across all objectives, preventing the generator from exploiting any single dimension.

Training Objectives

The total training loss drives adversarial interaction and joint optimization of the generator (Actor π_{θ}) and multi-objective reward model (Critic r_{ϕ}):

$$L = L_{\text{actor}} + L_{\text{critic}} \quad (25)$$

This loss formulation enables the Actor to generate high-quality, preference-aligned trajectories while the Critic refines its reward evaluation, fostering their collaborative evolution. Detailed component definitions are in the appendix.

Method	NC	DAC	EP	TTC	C	PDMS
Transfuser†(Chitta et al. 2022)	97.7	92.8	79.2	92.8	100	84.0
UniAD†(Hu et al. 2023)	97.8	91.9	78.8	92.9	100	83.4
PARA-Drive†(Weng et al. 2024)	97.9	92.4	79.3	93.0	99.8	84.0
VADv2†(Jiang et al. 2023)	97.9	91.7	77.6	92.9	100	83.0
LAW†(Li et al. 2024a)	96.4	95.4	81.7	88.7	99.9	84.6
DRAMA†(Yuan et al. 2024)	98.0	93.1	80.1	94.8	100	85.5
DiffusionDrive†(Liao et al. 2025)	98.2	96.2	82.2	94.7	100	88.1
Hydra-MDP†(Li et al. 2024b)	98.3	96.0	78.7	94.6	100	86.5
Hydra-MDP‡(Li et al. 2024b)	98.4	97.8	86.5	93.9	100	90.3
Hydra-MDP§(Li et al. 2024b)	98.4	97.7	85.0	94.5	100	89.9
DriveSuprim†(Yao et al. 2025)	97.8	97.3	86.7	93.6	100	89.9
DriveSuprim‡(Yao et al. 2025)	98.0	98.2	90.0	94.2	100	92.1
DriveSuprim§(Yao et al. 2025)	98.6	98.6	91.3	95.5	100	93.5
TrajHF†(GRPO)(Li et al. 2025a)	98.6	98.6	91.3	95.5	100	94.0
EvaDrive†(Cons)(Ours)	98.9	98.6	90.5	96.4	100	93.5
EvaDrive†(Aggres.)(Ours)	98.9	<u>98.5</u>	93.9	<u>96.2</u>	100	94.9

Table 1: Open-loop Results with Closed-loop Metrics on NAVSIMv1 Benchmark. Rows with **Cons**, and **Aggres.** denote EvoDrive under conservative and aggressive driving styles respectively. †: ResNet34; ‡: V2-99; §: ViT-L

Method	SR	DS	Effi.	Comf.
AD-MLP(Zhai et al. 2023)	0.00	18.05	48.45	22.63
UniAD(Hu et al. 2023)	16.36	45.81	129.21	43.58
VAD(Jiang et al. 2023)	15.00	42.35	157.94	46.01
TCP(Wu et al. 2022)	30.00	59.90	76.54	18.08
ThinkTwice(Jia et al. 2023b)	31.23	62.44	69.33	16.22
DriveAdapter(Jia et al. 2023a)	33.08	64.22	70.22	16.01
DriveTransformer(Jia et al. 2025)	35.01	65.02	100.64	20.78
EvaDrive(Aggres.)(Ours)	40.45	64.96	130.21	18.80

Table 2: Closed-loop Results on Bench2Drive Benchmark. Abbreviations: SR = Success Rate, DS = Driving Score, Effi. = Efficiency, Comf. = Comfortness.

Experiments

Due to space constraints, we present the **three core experiments**; more experimental tables can be found in the appendix.

Implementation Details

Experiments are conducted on the NAVSIM (Dauner et al. 2024), including open-loop evaluations on NAVSIM v1 (PDMS metric) and v2 (EPDMS metric) using real-world data, as well as closed-loop simulation on Bench2Drive via CARLA (Dosovitskiy et al. 2017). Our model uses a ResNet34 as backbone, MLP-based ego state encoders and reward models, and a 3-camera setup. Training is performed

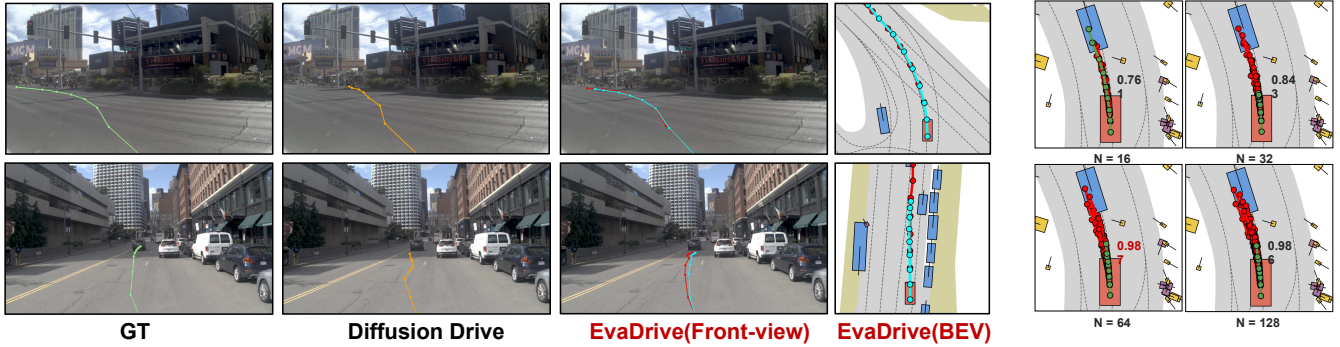


Figure 4: Visualization of end-to-end planning trajectories on Front-view and Bird-eye-view. Left (4a): Qualitative Comparison of Ground Truth, DiffusionDrive, and EvaDrive on NAVSIM NavTest Split (For EvaDrive: **red** denotes the aggressive version; **cyan** denotes our conservative version). Right (4b): Anchor visualization in each iteration (num=64): Red: constructed Pareto solution sets, gray: other eliminated anchors.

Variant	Modules				APO	PDMS
	2-Stage Generator	Multi-Object. Reward	Multi-Turn	Pareto Guidance		
(S0)	X	X	X	X	X	83.1
(S1)	✓	X	X	X	X	88.1
(S2)	✓	✓	X	X	X	91.7
(S3)	✓	✓	✓	X	X	93.7
(S4)	✓	✓	✓	✓	X	94.2
(S5)	✓	✓	✓	✓	✓	94.9

Table 3: Roadmap-based ablation study of EvaDrive. Modules are incrementally added.

on 4 NVIDIA H20 GPUs with Adam(Kingma and Ba 2014) optimizer (batch size 8 per GPU, learning rate 7.5×10^{-5}), alternating 5-epoch cycles between generator and critic for 30 epochs. Dataset and metric details are in the appendix.

Quantitative and Qualitative Comparison

Quantitative Analysis. Table 1 shows that EvaDrive achieves state-of-the-art results on NAVSIM v1, reaching 94.9 PDMS—surpassing DiffusionDrive(Liao et al. 2025) by 6.8, DriveSuprim(Yao et al. 2025) by 5.0, and TrajHF by 0.9 without relying on external preference data. By tuning the weight vector $\mathbf{w} = \{w_i\}_{i=1}^N$, we implement diverse driving styles, including conservative (favoring safety, low EP) and aggressive (higher EP, proactive behaviors). On Bench2Drive in CARLA, EvaDrive attains a Driving Score of 64.96 (Table 2), validating its closed-loop capability.

Qualitative Analysis. Figure 4a compares trajectories from GT, DiffusionDrive(Liao et al. 2025), and EvaDrive. Unlike the fixed behaviors of baselines, EvaDrive exhibits smooth transitions between conservative and aggressive modes via adjusting w , without manual rules. Figure 4b further illustrates the evolution of Pareto front size and distribution over iterations, highlighting the ability to explore diverse, high-quality solutions in the multi-objective space.

Roadmap Ablation

To systematically evaluate key components in *EvaDrive*, we conduct a roadmap-style ablation study. Starting from a basic imitation learning baseline (**S0**), we incrementally introduce the two-stage generator, multi-objective reward model, multi-turn optimization, Pareto front guidance, and adversarial preference optimization. Table 3 summarizes each module’s impact on planning performance over the NAVSIM v1 benchmark. Additional ablation results and analyses are provided in the appendix.

S1: Introducing the *two-stage generator* significantly improves trajectory smoothness and spatial diversity (+5.0 PDMS). The autoregressive stage captures temporal intent, while the diffusion-based refiner enhances spatial flexibility.

S2: Building upon S1, we incorporate a multi-objective reward model encoding diverse criteria (e.g., collision, acceleration, ego-progress) as explicit signals. This enables fine-grained trade-offs between comfort and efficiency, boosting PDMS to 91.7.

S3: Adding *multi-turn optimization* enables iterative refinement via historical feedback, enhancing robustness through continuous correction and reducing local optima (+2.0 PDMS vs. S2, reaching 93.7).

S4: *Pareto front guidance* preserves optimal trade-offs across objectives, promoting diverse yet high-quality solutions and achieving a PDMS of 94.2.

S5: *Adversarial preference optimization* enhances policy quality by training reward-aware discriminators to refine the actor via feedback, yielding the highest PDMS of **94.9**.

Conclusion

This paper presents **EvaDrive**, a multi-objective RL planner unifying generation and evaluation via adversarial co-evolution. Drawing on human decision-making, it uses multi-round Pareto optimization with a structured non-scalar reward model to maintain trajectory diversity while avoiding scalarization bias and annotation noise. Combining a hierarchical generator, diffusion-based refinement, and critic, EvaDrive enables precise control over trajectory semantics, diversity, and safety. Evaluated on NAVSIM and

Bench2Drive, it achieves 94.9 PDMS and 64.96 Driving Score, positioning EvaDrive as the first closed-loop planner for scalarization-free, preference-aware trajectory optimization in both open- and closed-loop settings.

Appendix

Further Related Works

E2E AD

Imitation learning (IL) has been widely adopted for E2E trajectory planning in autonomous driving, where raw sensor inputs are mapped to expert demonstrations (Shao et al. 2023; Qian et al. 2024a, 2025b). UniAD (Hu et al. 2023), Transfuser (Chitta et al. 2022) leverage Bird-Eye-View (BEV) representations and introduce unified multi-task and safety-aware architectures to build planning-centric frameworks. VAD (Jiang et al. 2023) further improve this design by employing query-based representations and constructing a trajectory vocabulary, effectively transforming the problem from regression into a discrete classification task.

To model the interactions between the ego vehicle and other traffic participants, GenAD (Zheng et al. 2024) and PPAD (Chen et al. 2024b) utilize instance-level visual features, while GraphAD (Zhang et al. 2024) represents these features as nodes in a graph structure. SparseDrive (Sun et al. 2024) propose a fully sparse architecture, achieving greater efficiency and superior planning performance. However, most of these methods typically rely on constructing heavy BEV features, which prevents downstream tasks from learning directly from raw sensor data.

To address this issue, PARA-Drive (Weng et al. 2024) and DriveTransformer (Jia et al. 2025) introduce a parallel pipeline, enabling a more unified and scalable framework for end-to-end driving systems. Additionally, methods such as AD-MLP (Zhai et al. 2023) adopt a simple network architecture and are tested on nuScenes (Caesar et al. 2020), relying solely on the ego vehicle’s status information. These approaches highlight the potential over-reliance on ego status in simpler driving scenarios while also revealing limitations in the effective use of perception data. Recent benchmarks like NavSim (Dauner et al. 2024) advance E2E planning with multi-agent scenarios, while frameworks including Hydra-MDP (Li et al. 2024b), GTRS (Li et al. 2025c) and iPad (Guo et al. 2025) employ scorer-based trajectory synthesis integrating environmental interactions. However, these universally lack generator-scorer feedback loops. Contrastingly, our human decision-inspired solution integrates trajectory generation and evaluation within an iterative optimization cycle.

RL in generative task(multi-object and multi-turn)

RL has emerged as a critical paradigm for optimizing generative models in complex, goal-driven scenarios, particularly in multi-objective and multi-turn dialogue systems(Ouyang et al. 2022; Zhou et al. 2025; Shani et al. 2024). These tasks require balancing competing objectives (e.g., fluency, coher-

ence, task success) and maintaining long-term context consistency across multiple interaction turns.

Key challenges include non-differentiable reward engineering, sparse-reward exploration-exploitation tradeoffs, and cross-user generalization. Emerging solutions integrate LLMs for reward modeling (Ouyang et al. 2022) and offline RL to reduce interaction costs (Gupta et al. 2023), while hybrid methods with pretrained dialogue systems (Yang, Li, and Quan 2021) balance task efficiency with natural fluency. In autonomous driving, post-training alignment methods like GRPO (Shao et al. 2024) and DPO (Rafailov et al. 2023) optimize human preference matching. Contrastingly, our framework pioneers multi-round multi-objective RL with Adversarial Policy Optimization (APO) (Cheng et al. 2023) for trajectory optimization.

GAN in generative task

Generative Adversarial Networks (GANs) have emerged as a cornerstone of modern generative modeling, enabling the synthesis of high-quality, realistic data across modalities(Goodfellow et al. 2014). Their adversarial training framework, comprising a generator and discriminator in a minimax game, has driven breakthroughs in image generation(Karrast et al. 2018), text-to-image synthesis(Kang et al. 2023), and domain adaptation(Zhu et al. 2017).

In autonomous driving, GANs address critical challenges in data scarcity, sensor simulation, and domain adaptation. First, they generate synthetic sensor data (e.g., RGB-D) to augment training datasets. CycleGAN(Zhu et al. 2017) has been adapted to translate daytime images to nighttime abstractscenes for robust perception under varying lighting conditions(Yang et al. 2020). SocialGAN (Gupta et al. 2018) integrates adversarial training for pedestrian motion forecasting. Physics-informed GANs like PhySGAN (Kong et al. 2020) enforce physical consistency in simulated sensor outputs by incorporating collision dynamics, reducing the simulation-to-reality gap. This paper integrates GANs into a reinforcement learning framework for autonomous driving, addressing critical gaps in trajectory planning research.

Further Loss Function Detail

Training Objectives

To jointly optimize the **generator (Actor)** and the **multi-objective reward model (Critic)**, we formulate a structured loss design. We emphasize a **multi-objective design philosophy**: each reward dimension reflects a distinct aspect of trajectory quality (e.g., safety, comfort, efficiency). To accommodate this, we introduce a **normalized weight vector** $\{w_i\}_{i=1}^N$, with $w_i \geq 0$ and $\sum_i w_i = 1$, enabling adaptive emphasis on different trajectory qualities. These weights can be either manually defined or learned during training, as discussed later.

Actor Loss (L_{actor})

The Actor π_θ aims to generate high-quality trajectories that are not only feasible but also align with desired behavioral preferences. The loss consists of three components:

(1) Imitation Loss. The **imitation loss** encourages the Actor π_θ to mimic expert demonstrations. This is implemented as a supervised loss over state-action pairs, specifically using the **Binary Cross-Entropy (BCE) loss**, formulated as:

$$L_{\text{imitation}} = \mathbb{E}_{(s,a) \sim \pi_{\text{expert}}} [\text{BCE}(\pi_\theta(a|s), a)]. \quad (26)$$

Here, s denotes the **state**, a denotes the **action**, $\pi_\theta(a|s)$ is the Actor’s predicted action distribution given state s , and π_{expert} represents the **expert policy**.

(2) Diversity Loss. To mitigate mode collapse and promote exploration, we add a **diversity loss** that penalizes semantic redundancy among generated trajectories within the same batch. We encourage the policy to cover a broader distribution by **minimizing mutual information**:

$$L_{\text{diversity}} = \mathbb{E}_{\tau_i, \tau_j \sim \pi_\theta, i \neq j} [\text{MI}(\tau_i, \tau_j)], \quad (27)$$

where τ_i and τ_j are **distinct trajectories** generated by the Actor π_θ , and $\text{MI}(\cdot, \cdot)$ denotes **mutual information**, used to measure the redundancy between encodings of two trajectories.

(3) Adversarial Preference Loss. This is a key innovation: we formulate trajectory generation as a **multi-objective reward maximization problem**, using a learned reward model $r_\phi^{(i)}(s, a)$ for each dimension. The Actor seeks to generate trajectories that maximize cumulative reward across all dimensions:

$$L_{\text{adv, actor}} = -\mathbb{E}_{(s,a) \sim \pi_\theta} \left[\sum_{i=1}^N w_i r_\phi^{(i)}(s, a) \right] + \lambda \cdot \text{KL}(\pi_\theta \| \pi_{\text{ref}}). \quad (28)$$

Here, $r_\phi^{(i)}(s, a)$ is the Critic model’s predicted reward for the state-action pair (s, a) on the i -th **reward dimension**, and N is the **total number of reward dimensions**. λ is the **KL regularization coefficient**, and $\text{KL}(\pi_\theta \| \pi_{\text{ref}})$ is the **KL divergence** between the Actor’s policy π_θ and a **reference policy** π_{ref} , used to stabilize training by constraining deviations from the reference policy.

Flexible Objective Control: We attempted to parameterize the weights $\{w_i\}$ and optimize them through training, but the results were unsatisfactory. The model tended to directly adjust the weights in directions that made loss reduction easier, ultimately leading to mode collapse. Therefore, we switched to manually designing several different weight configurations; relevant experimental data can be found in Table 7.

Final Actor Objective:

$$L_{\text{actor}} = L_{\text{imitation}} + L_{\text{diversity}} + L_{\text{adv, actor}}. \quad (29)$$

Critic Loss (L_{critic})

The Critic, a **multi-objective reward model** $r_\phi = \{r_\phi^{(i)}\}_{i=1}^N$, is trained to evaluate the quality of trajectories along distinct reward dimensions. Its loss includes:

(1) Reward Supervision Loss. When ground-truth or human-labeled reward signals are available, we use a supervised regression loss to train each reward head. This term explicitly employs the **Binary Cross-Entropy (BCE) loss**:

$$L_{\text{reward}} = \mathbb{E}_{(s,a)} \left[\sum_{i=1}^N \text{BCE} \left(r_\phi^{(i)}(s, a), r_{\text{gt}}^{(i)}(s, a) \right) \right], \quad (30)$$

where $r_\phi^{(i)}(s, a)$ is the Critic model’s predicted reward on the i -th **dimension**, and $r_{\text{gt}}^{(i)}(s, a)$ is the **ground-truth reward signal for the i -th dimension**. This term anchors the Critic’s predictions in observable feedback, consistent with the “BCE loss” paradigm in reinforcement learning.

(2) Adversarial Alignment Loss. In the adversarial loop, the Critic is optimized to distinguish expert trajectories from generated ones in the multi-dimensional reward space:

$$L_{\text{adv, critic}} = \mathbb{E}_{(s,a) \sim \pi_\theta} \left[- \sum_{i=1}^N w_i r_\phi^{(i)}(s, a) \right] \quad (31)$$

$$+ \mathbb{E}_{(s,a) \sim \pi_{\text{expert}}} \left[\sum_{i=1}^N w_i r_\phi^{(i)}(s, a) \right]$$

$$+ \beta \cdot \text{KL}(P_{\text{expert}} \| Q_\phi), \quad (32)$$

where β is the **KL regularization coefficient**, P_{expert} is the **reward distribution of expert trajectories**, and Q_ϕ denotes the **Critic-induced distribution over preferences**. The KL regularization prevents overfitting to the expert dataset.

Final Critic Objective:

$$L_{\text{critic}} = L_{\text{reward}} + L_{\text{adv, critic}}. \quad (33)$$

This collaborative training scheme establishes a dynamic interplay between Actor and Critic: the Actor generates trajectories to maximize multi-dimensional rewards, while the Critic continually refines its judgment to distinguish superior behaviors. This adversarial preference optimization drives the model to explore high-reward, diverse, and controllable behaviors across iterations. The overall training objective is defined as a combination of actor and critic losses:

$$L = L_{\text{actor}} + L_{\text{critic}}. \quad (34)$$

Further Visualization Results

We present additional visualization results. Figure 5 shows comparative visualizations of our method, ground truth (GT), and DiffusionDrive across more road scenarios, demonstrating the consistency of our approach in diverse environmental conditions. Figure 6 visualizes the trajectory candidates generated by our model and the constructed Pareto frontier. These visualizations further validate the effectiveness and rationality of our method in practical driving scenarios.

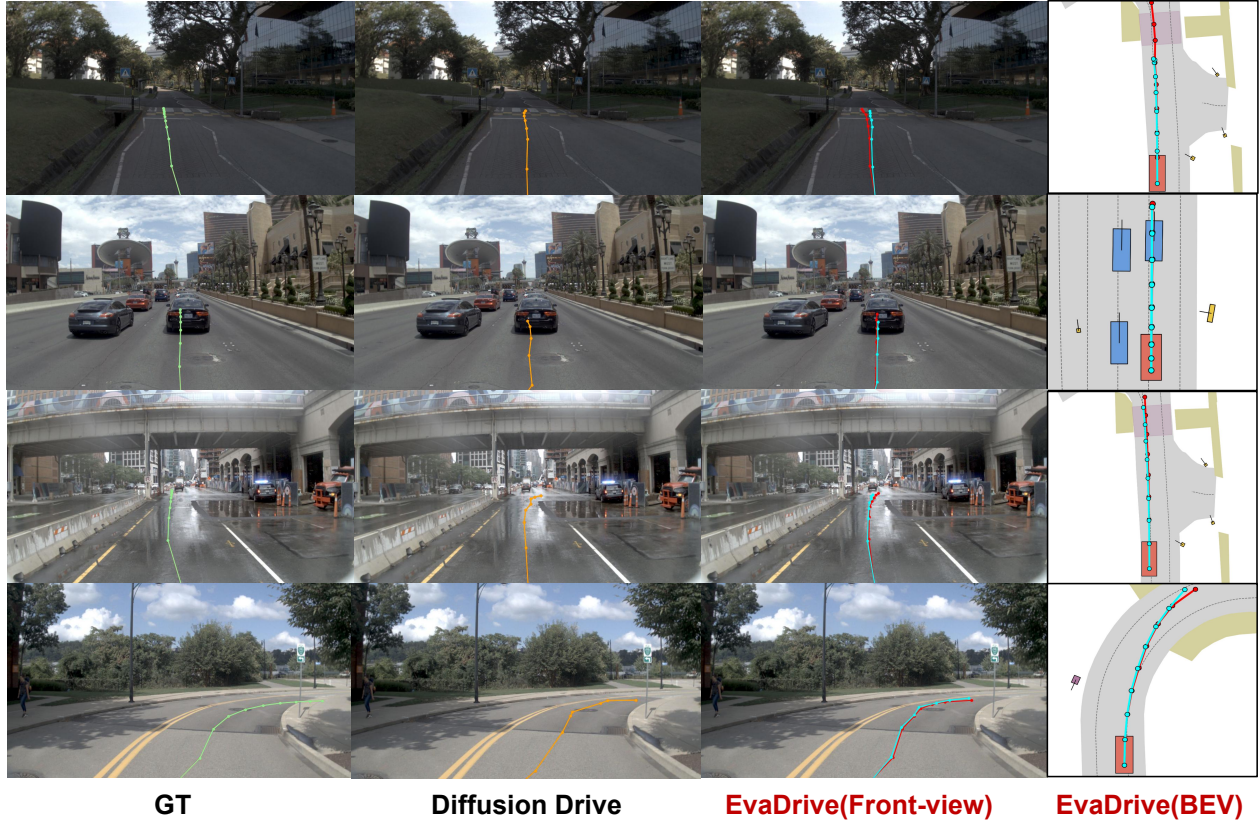


Figure 5: Comparative visualizations of ground truth, DiffusionDrive, and our method trajectories across diverse road scenarios (urban intersections, highway merges) on front camera views.

Further Experiment Settings

Implementation Details

Dataset and Metrics We conduct experiments mainly on the NAVSIM [9] benchmark, which is a driving dataset containing challenging driving scenarios. There are two different evaluation metrics on NAVSIM, leading to NAVSIMv1 and NAVSIMv2. The evaluation metric of NAVSIMv1 is the **PDM Score (PDMS)**. Each predicted trajectory is sent to a simulator to collect different rule-based subscores, which are aggregated to get the final PDMS:

$$\text{PDMS} = \frac{\prod_{m \in SP} \text{score}_m \times \sum_{w \in SA} \text{weight}_w \times \text{score}_w}{\sum_{w \in SA} \text{weight}_w} \quad (35)$$

Further Experiment Settings

where SP and SA denote the penalty subscore set and the weighted average subscore set. In NAVSIMv1, SP comprises two subscores, including **no collisions (NC)** and **drivable area compliance (DAC)**, and SA comprises **ego progress (EP)**, **time-to-collision (TTC)**, and **comfort (C)**. For NAVSIM, we use the official log-replay simulator with an LQR controller operating at 10 Hz over a 4-second horizon, with detailed sub-metric definitions as follows:

- **NoAt-Fault Collision (NC)**: Set to 0 if, at any simulation step, the proposal’s bounding box intersects with other road users (vehicles, pedestrians, or bicycles). Collisions not considered “at-fault” in non-reactive environments (e.g., ego vehicle stationary) are ignored; collisions with static objects apply a softer penalty of 0.5.
- **Drivable Area Compliance (DAC)**: Set to 0 if any corner of the proposal state lies outside drivable area polygons at any step.
- **Time-to-Collision (TTC)**: Initialized to 1, set to 0 if projected TTC (assuming constant velocity/heading) drops below 1 second within the 4-second horizon.
- **Comfort (C)**: Set to 0 if motion exceeds thresholds: lateral acceleration $> 4.89 \text{ m/s}^2$, longitudinal acceleration $> 2.40 \text{ m/s}^2$, longitudinal deceleration $> 4.05 \text{ m/s}^2$, absolute jerk $> 8.37 \text{ m/s}^3$, longitudinal jerk $> 4.13 \text{ m/s}^3$, yawrate $> 0.95 \text{ rad/s}$, or yaw acceleration $> 1.93 \text{ rad/s}^2$.
- **Ego Progress (EP)**: Measures progress along the route center, normalized by a safe upper bound from the PDM-Closed planner. The ratio is clipped to $[0,1]$, with scores discarded if the upper bound > 5 meters or progress is negative.

NAVSIMv2 introduces 4 additional subscores: **driving**



Figure 6: Visualization of model-generated trajectory candidates (gray lines) and the Pareto frontier in red, highlighting optimal safety-efficiency-comfort trade-offs.

direction compliance (DDC) and **traffic light compliance (TLC)** are added to the penalty sub-score set (SP), while **lanekeeping (LK)** and **extended comfort (EC)** are included in the weighted average sub-score set (SA). Additionally, the original comfort sub-score is revised and renamed as **history comfort (HC)**. Aggregating all these sub-scores yields the **EPDMS** metric specific to NAVSIMv2. Table 4 presents the performance of our method on the NAVSIMv2 benchmark.

We also evaluate on the Bench2Drive benchmark, utilizing Carla simulator with a perfect controller operating at 2 Hz over a 3-second horizon. Its evaluation sub-metrics include:

- **NoCollision (NC)**: Set to 0 if the proposal’s bounding box intersects with any object (vehicles, bicycles, pedestrians, traffic signs, cones, or lights) at any step.
- **Drivable Area Compliance (DAC)**: Set to 0 if any corner of the proposal state is off-road or all centers are off-route at any step.
- **Time-to-Collision (TTC)**: Set to 0 if projected TTC drops below 1 second within the 3-second horizon.
- **Comfort**: Set to 0 if acceleration or turning rate exceeds the expert trajectory’s maximum values.
- **Ego Progress**: Defined as the ratio of ego progress along the expert trajectory (conditioned on collision-free and on-road status). If the ratio exceeds 1, its reciprocal is used.

Model Details Our method employs a ResNet34 backbone as the image encoder Enc_i . Input images are resized to a resolution of 2048×512 . We use a two-layer MLP (Multi-Layer Perceptron) to encode the ego-vehicle state and the high-scoring trajectories returned by the critic, with the encoded results used for anchor initialization. Another two-layer MLP is adopted as the reward model, followed by a linear layer to predict all metrics.

The number of candidate trajectories per round is set to 64, and the Pareto frontier is constructed using the **Fast Non-Dominated Sorting algorithm** (see Algorithm 2 for details on frontier construction and differentiable injection). The process involves: first, ranking the 64 candidate trajectories into hierarchical levels based on multi-objective metrics to form solution sets with different dominance ranks; then selecting the highest-ranked non-dominated solution set as the current Pareto frontier, with diversity maintained via crowded distance calculation to prevent local concentration. After construction, Gumbel-Softmax sampling injects frontier solutions into the previous round’s trajectory candidates, ensuring full differentiability throughout training.

For perception input, we adopt a three-camera FOV setup, with images sourced from the $l0$ (left), f (front), and $r0$ (right) cameras.

Training Details We train our model on 4 NVIDIA H20 GPUs using a **generative-adversarial approach**. We adopt the **Adam optimizer** for model training, with the batch size on a GPU set to 8, and the learning rate at 7.5×10^{-5} . Our

Algorithm 2: Differentiable Fast Non-dominated Sorting with Gumbel-Softmax Sampling

Input: Candidate trajectories $\mathcal{A} = \{a_i\}_{i=1}^{64}$, reward vectors $\{\mathbf{r}(a_i)\}_{i=1}^{64}$

Output: Sampled trajectories $\{\tilde{a}^{(m)}\}_{m=1}^M$ for differentiable guidance

1. Fast non-dominated sorting

Initialize $n_i \leftarrow 0$, $S_i \leftarrow \emptyset$, $\mathcal{F}_1 \leftarrow \emptyset$;

foreach $a_i \in \mathcal{A}$ **do**

foreach $a_j \in \mathcal{A}$ **do**

if $\mathbf{r}(a_i) \succ \mathbf{r}(a_j)$ **then** $S_i \leftarrow S_i \cup \{a_j\}$;

else if $\mathbf{r}(a_j) \succ \mathbf{r}(a_i)$ **then** $n_i \leftarrow n_i + 1$;

if $n_i = 0$ **then** $r_i \leftarrow 1$, $\mathcal{F}_1 \leftarrow \mathcal{F}_1 \cup \{a_i\}$;

$k \leftarrow 1$;

while $\mathcal{F}_k \neq \emptyset$ **do**

$\mathcal{Q} \leftarrow \emptyset$;

foreach $a_i \in \mathcal{F}_k$ **do**

foreach $a_j \in S_i$ **do**

$n_j \leftarrow n_j - 1$;

if $n_j = 0$ **then** $r_j \leftarrow k + 1$,

$\mathcal{Q} \leftarrow \mathcal{Q} \cup \{a_j\}$;

$k \leftarrow k + 1$, $\mathcal{F}_k \leftarrow \mathcal{Q}$;

2. Extract Pareto front $\mathcal{P} \leftarrow \mathcal{F}_1$;

3. Compute crowding distance

$\{d(a)\}_{a \in \mathcal{P}} \leftarrow \text{CrowdingDistance}(\mathcal{P})$;

4. Gumbel-Softmax sampling from \mathcal{P}

 Compute logits $\ell(a) \propto d(a)$ for $a \in \mathcal{P}$;

for $m = 1$ **to** M **do**

$\tilde{a}^{(m)} \sim \text{GumbelSoftmaxSample}(\{\ell(a)\}_{a \in \mathcal{P}})$;

return $\{\tilde{a}^{(m)}\}_{m=1}^M$;

training strategy involves **alternating optimization cycles** between the generator and the critic. Specifically, the generator is trained for 5 epochs, followed by the critic for 5 epochs. This 5-epoch cycle is repeated alternately, for a total of **30 training epochs**.

Further Ablation Studies

Reward Structures and Optimization Strategies

To better understand the individual contributions of reward modeling and optimization mechanisms in our framework, we conduct a comprehensive ablation study covering both single-objective and multi-objective reinforcement learning paradigms. We distinguish methods along two axes: the *reward type* (i.e., whether the policy is trained using a scalar objective or a structured reward vector), and the *optimization strategy* (e.g., vanilla policy gradient, preference-based optimization, or our adversarial policy optimization paradigm).

Table 5 summarizes the results in terms of PDMS, a holistic driving quality metric. As seen, the baseline method **PPO (Scalarized)** adopts manually weighted scalar rewards and uses standard policy optimization. Despite being simple and widely used, it fails to balance safety and comfort, resulting in the lowest PDMS.

We also evaluate **TrajHF**, a GRPO-style method which learns a scalar reward via pairwise preference rankings. Although it improves slightly over scalarized PPO, its scalar reward structure fundamentally limits its ability to represent multi-dimensional planning objectives. Therefore, we categorize TrajHF as a *single-objective* RL method, despite the use of preference-based supervision.

To isolate the effect of multi-objective rewards, we compare with **EvaDrive (w/o APO)**, which leverages structured reward vectors but optimizes the policy without adversarial co-evolution or Pareto-guided feedback. This variant already shows notable gains, indicating that vectorized reward modeling improves alignment with planning principles.

Finally, our full framework **EvaDrive (APO)** achieves the best performance, demonstrating the synergy between structured reward modeling, adversarial optimization, and multi-turn Pareto-guided feedback. These results highlight that each component—multi-objective formulation, co-evolutionary training, and Pareto supervision—plays a complementary and indispensable role.

Number of Multi-Round Iterations

Table 6 investigates the impact of iteration counts on planning performance. Experimental results show that our method can achieve satisfactory planning quality even with a single iteration; performance reaches its optimal level at 2–3 iterations, but slightly degrades when the iteration count increases to 4 or more.

Specifically, excessive iterations tend to cause two issues: first, the model may over-focus on fine-tuning local trajectory details, neglecting the rationality of the global path; second, as the number of iterations increases, the diversity of trajectory candidate sets gradually diminishes, with higher similarity among high-quality solutions, making it difficult to cover potential optimal solutions in complex scenarios. Meanwhile, cumulative errors in the computation process gradually amplify, ultimately leading to slight performance degradation.

Considering the trade-off between planning performance and computational efficiency (excessive iterations significantly increase inference time), we select 2 iterations as the default setting.

Preference Weight Balancing

Table 7 presents the experimental results of trajectory generation under different weight configurations for reward signal dimensions, verifying the model’s adaptability to diverse preference settings.

We first attempted to parameterize the weight matrix $\{w_i\}_{i=1}^N$ and allow the model to learn it autonomously, but this approach yielded poor performance. The core issue lies in inherent flaws in the autonomous optimization: during training, the model exploits loss landscape asymmetry, prioritizing dimensions where loss reduction is computationally easy (e.g., minor tweaks to comfort or progress metrics) while neglecting critical but hard-to-optimize dimensions (e.g., safety metrics requiring complex trajectory adjustments). This short-sighted focus on immediate loss minimization leads to reward collapse—the model gradually sac-

Method	Backbone	NC \uparrow	DAC \uparrow	DDC \uparrow	TL \uparrow	EP \uparrow	TTC \uparrow	LK \uparrow	HC \uparrow	EC \uparrow	EPDMS \uparrow
Human Agent	—	100	100	99.8	100	87.4	100	100	98.1	90.1	90.3
EgoStatusMLP	—	93.1	77.9	92.7	99.6	86.0	91.5	89.4	98.3	85.4	64.0
Transfuser[7]	ResNet34	96.9	89.9	97.8	99.7	87.1	95.4	92.7	98.3	87.2	76.7
HydraMDP++[27]	ResNet34	97.2	97.5	99.4	99.6	83.1	96.5	94.4	98.2	70.9	81.4
HydraMDP++[27]	V2-99	98.4	98.0	99.4	99.8	87.5	97.7	95.3	98.3	77.4	85.1
HydraMDP++[27]	ViT-L	98.5	98.5	99.5	99.7	87.4	97.9	95.8	98.2	75.7	85.6
DriveSuprim	ResNet34	97.5	96.5	99.4	99.6	88.4	96.6	95.5	98.3	77.0	83.1
DriveSuprim	V2-99	97.8	97.9	99.5	99.9	90.6	97.1	96.6	98.3	77.9	86.0
EvoDrive(Aggres.)	ResNet34	98.8	98.5	98.9	99.8	96.6	98.4	94.3	97.8	55.9	86.3

Table 4: Evaluation on NAVSIM v2. Results are grouped by methods.

Method	Reward Type	Optimization Method	PDMS \uparrow
PPO (Scalarized)	Single-objective	PPO	91.7
TrajHF (GRPO-style)	Single-objective	GRPO	94.0
EvaDrive (w/o APO)	Multi-objective	PPO	93.5
EvaDrive (Full)	Multi-objective	APO	94.9

Table 5: Ablation on reward structures and optimization strategies. Performance comparisons under different conditions (NAVSIM Benchmark)

Iterations	PDMS	Time(ms)	Avg. Pareto Size	Avg. Crowding Distance
1 (Single)	93.1	45	-	-
2	94.9	69	8.5	12.3
3	94.8	104	6.1	9.3
4	93.6	145	3.2	5.5

Table 6: EvaDrive vs. Iterations (Performance comparisons under different conditions)

Preference	NC	DAC	EP	TTC	C	PDMS
Weight Parameterization (Self-Learned)	89.3	90.1	76.5	88.2	91.7	87.2
Conservative (0.4:0.2:0.2:0.1:0.1)	99.1	98.8	87.2	97.1	100	93.5
Balanced (0.2:0.2:0.2:0.2:0.2)	98.9	98.5	91.9	96.2	100	94.2
Aggressive (0.1:0.4:0.1:0.2:0.2)	98.7	97.9	93.3	95.8	100	94.9
Comfort-focused (0.2:0.2:0.4:0.1:0.1)	99.0	98.2	89.0	96.5	100	94.0

Table 7: Performance Comparisons Under Different Preference Weights (Safety:Efficiency:Comfot:EgoProgress:CollisionAvoidance) on NAVSIM Benchmark. Subscores include No Collisions (NC), Drivable Area Compliance (DAC), Ego Progress (EP), Time-to-Collision (TTC), and Comfort (C).

Experimental Setup	NC	DAC	TTC	C	EP	PDMS
No stages (baseline)	97.8	95.2	94.0	99.5	81.5	83.1
Only Stage 1	98.0	95.6	94.2	99.6	81.8	85.6
Only Stage 2	98.2	96.3	94.6	99.8	82.0	87.0
Reversed order (Stage 2 → Stage 1)	97.9	95.8	94.3	99.7	82.2	85.9
Our design (Stage 1 → Stage 2)	98.3	96.5	94.8	100	83.3	88.1

Table 8: Ablation study on Two-Stage Actor Design (NAVSIM Benchmark). "Stage 1 → Stage 2" denotes our proposed sequential architecture, while "Stage 2 → Stage 1" represents reversed module order.

Config	NC	DAC	TTC	C	EP	PDMS
16	97.2	93.0	92.5	99.0	89.3	90.5
32	98.0	95.9	94.5	99.7	93.3	92.9
64	98.6	96.3	95.0	100	93.2	94.85
128	98.6	96.4	95.1	100	91.3	94.85

Table 9: Ablation study on Anchor Number (NAVSIM Benchmark)

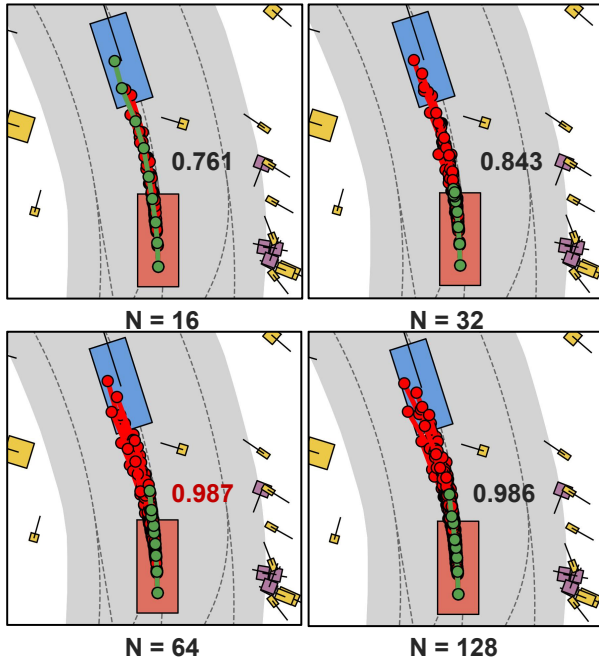


Figure 7: Relationship between the number of anchors and trajectory scores. The scores in the figure represent the score of a single trajectory.

rifices key characteristics to simplify optimization, degrading performance across core evaluation criteria. Fundamentally, the optimization process lacks mechanisms to ensure balanced attention to all critical dimensions, causing it to favor loss reduction shortcuts over robust performance.

The **Conservative** setting employs a weight distribu-

tion (0.4:0.2:0.1:0.2:0.1 for NC:DAC:EP:TTC:C), prioritizing safety via higher weights for no-collision (NC) and drivable area compliance (DAC) subscores. This configuration emphasizes collision avoidance and strict adherence to drivable areas, reflecting a risk-averse strategy that places safe operation above route progress (EP).

In contrast, the **Aggressive** configuration (0.1:0.2:0.4:0.1:0.2 for NC:DAC:EP:TTC:C) shifts focus to efficiency by significantly increasing the weight of ego progress (EP) to prioritize route advancement. This setup deliberately trades moderate reductions in safety metrics (NC, TTC) for faster route completion efficiency.

The **Balanced** weights (0.2:0.2:0.2:0.2:0.2) distribute importance equally across all subscores (no collisions, drivable area compliance, ego progress, time-to-collision, and comfort), avoiding extreme prioritization of any single aspect and achieving stable, balanced performance across evaluation criteria.

Notably, the **Comfort-focused** setting (0.2:0.2:0.1:0.1:0.4 for NC:DAC:EP:TTC:C) assigns the highest weight to comfort (C), explicitly prioritizing smooth driving characteristics (e.g., acceleration and jerk constraints). It retains baseline weights for safety (NC, DAC) and progress (EP) to ensure improved comfort does not come at the cost of significant sacrifices in these areas, validating the model's adaptability to explicit comfort preferences.

Design of Two-Stage Actor

Table 8 demonstrates the effectiveness of the stage-wise design module in our proposed Actor. Experimental results show that using only the autoregressive module or the diffusion module as the trajectory generator, or reversing the order of the two modules, all result in inferior performance compared to our designed architecture.

Anchor Number Configuration

We analyzed how anchor point count impacts trajectory quality (Table 9). The **16-anchor** setup performed poorest due to insufficient sampling density. Increasing to **32 anchors** yielded a notable PDMS jump to 92.9, with improved safety and efficiency. **64 anchors** further optimized performance (PDMS=94.9) with optimal safety and comfort, while **128 anchors** showed negligible gains, confirming 64 as the optimal balance of sampling density and computational efficiency.

References

- Caesar, H.; Bankiti, V.; Lang, A. H.; Vora, S.; Liong, V. E.; Xu, Q.; Krishnan, A.; Pan, Y.; Baldan, G.; and Beijbom, O. 2020. nuscenes: A multimodal dataset for autonomous driving. In *Proceedings of the IEEE/CVF conference on computer vision and pattern recognition*, 11621–11631.
- Chen, S.; Jiang, B.; Gao, H.; Liao, B.; Xu, Q.; Zhang, Q.; Huang, C.; Liu, W.; and Wang, X. 2024a. Vadv2: End-to-end vectorized autonomous driving via probabilistic planning. *arXiv preprint arXiv:2402.13243*.
- Chen, Z.; Ye, M.; Xu, S.; Cao, T.; and Chen, Q. 2024b. Ppad: Iterative interactions of prediction and planning for end-to-end autonomous driving. In *European Conference on Computer Vision*, 239–256. Springer.
- Cheng, P.; Yang, Y.; Li, J.; Dai, Y.; and Du, N. 2023. Adversarial preference optimization. *CoRR*.
- Chitta, K.; Prakash, A.; Jaeger, B.; Yu, Z.; Renz, K.; and Geiger, A. 2022. Transfuser: Imitation with transformer-based sensor fusion for autonomous driving. *IEEE transactions on pattern analysis and machine intelligence*, 45(11): 12878–12895.
- Dauner, D.; Hallgarten, M.; Li, T.; Weng, X.; Huang, Z.; Yang, Z.; Li, H.; Gilitschenski, I.; Ivanovic, B.; Pavone, M.; et al. 2024. Navsim: Data-driven non-reactive autonomous vehicle simulation and benchmarking. *Advances in Neural Information Processing Systems*, 37: 28706–28719.
- Dosovitskiy, A.; Ros, G.; Codevilla, F.; Lopez, A.; and Koltun, V. 2017. CARLA: An Open Urban Driving Simulator. In *Proceedings of the 1st Annual Conference on Robot Learning*, 1–16.
- Fu, Z.; Lin, H.; Qian, K.; Wen, T.; Gao, H.; Zhong, Z.; and Yang, D. 2025. Enhancing Autonomous Vehicle Planning With a Robust Fault-Tolerant Mechanism for Action-Induced Agent Detection. In *ICASSP 2025-2025 IEEE International Conference on Acoustics, Speech and Signal Processing (ICASSP)*, 1–5. IEEE.
- Goodfellow, I. J.; Pouget-Abadie, J.; Mirza, M.; Xu, B.; Warde-Farley, D.; Ozair, S.; Courville, A.; and Bengio, Y. 2014. Generative adversarial nets. *Advances in neural information processing systems*, 27.
- Guo, K.; Liu, H.; Wu, X.; Pan, J.; and Lv, C. 2025. iPad: Iterative Proposal-centric End-to-End Autonomous Driving. *arXiv preprint arXiv:2505.15111*.
- Gupta, A.; Johnson, J.; Fei-Fei, L.; Savarese, S.; and Alahi, A. 2018. Social gan: Socially acceptable trajectories with generative adversarial networks. In *Proceedings of the IEEE conference on computer vision and pattern recognition*, 2255–2264.
- Gupta, D.; Chow, Y.; Tulepbergenov, A.; Ghavamzadeh, M.; and Boutilier, C. 2023. Offline reinforcement learning for mixture-of-expert dialogue management. *Advances in Neural Information Processing Systems*, 36: 5912–5935.
- Hu, S.; Chen, L.; Wu, P.; Li, H.; Yan, J.; and Tao, D. 2022. St-p3: End-to-end vision-based autonomous driving via spatial-temporal feature learning. In *European Conference on Computer Vision*, 533–549. Springer.

- Hu, Y.; Yang, J.; Chen, L.; Li, K.; Sima, C.; Zhu, X.; Chai, S.; Du, S.; Lin, T.; Wang, W.; et al. 2023. Planning-oriented autonomous driving. In *Proceedings of the IEEE/CVF conference on computer vision and pattern recognition*, 17853–17862.
- Jia, X.; Gao, Y.; Chen, L.; Yan, J.; Liu, P. L.; and Li, H. 2023a. DriveAdapter: Breaking the Coupling Barrier of Perception and Planning in End-to-End Autonomous Driving. In *ICCV*.
- Jia, X.; Wu, P.; Chen, L.; Xie, J.; He, C.; Yan, J.; and Li, H. 2023b. Think Twice before Driving: Towards Scalable Decoders for End-to-End Autonomous Driving. In *CVPR*.
- Jia, X.; You, J.; Zhang, Z.; and Yan, J. 2025. DriveTransformer: Unified Transformer for Scalable End-to-End Autonomous Driving. In *International Conference on Learning Representations (ICLR)*.
- Jiang, B.; Chen, S.; Xu, Q.; Liao, B.; Chen, J.; Zhou, H.; Zhang, Q.; Liu, W.; Huang, C.; and Wang, X. 2023. Vad: Vectorized scene representation for efficient autonomous driving. In *Proceedings of the IEEE/CVF International Conference on Computer Vision*, 8340–8350.
- Jiang, B.; Chen, S.; Zhang, Q.; Liu, W.; and Wang, X. 2025a. Alphadrive: Unleashing the power of vlms in autonomous driving via reinforcement learning and reasoning. *arXiv preprint arXiv:2503.07608*.
- Jiang, S.; Huang, Z.; Qian, K.; Luo, Z.; Zhu, T.; Zhong, Y.; Tang, Y.; Kong, M.; Wang, Y.; Jiao, S.; et al. 2025b. A Survey on Vision-Language-Action Models for Autonomous Driving. *arXiv preprint arXiv:2506.24044*.
- Kang, M.; Zhu, J.-Y.; Zhang, R.; Park, J.; Shechtman, E.; Paris, S.; and Park, T. 2023. Scaling up gans for text-to-image synthesis. In *Proceedings of the IEEE/CVF conference on computer vision and pattern recognition*, 10124–10134.
- Karrast, T.; Ailat, T.; Laines, S.; et al. 2018. Progressive growing of GANs for improved quality, stability, and variation. In *Proceedings of the 6th International Conference on Learning Representations. Vancouver, Canada: Open Review. net*.
- Kingma, D. P.; and Ba, J. 2014. Adam: A method for stochastic optimization. *arXiv preprint arXiv:1412.6980*.
- Kiran, B. R.; Sobh, I.; Talpaert, V.; Mannion, P.; Al Sallab, A. A.; Yogamani, S.; and Pérez, P. 2021. Deep reinforcement learning for autonomous driving: A survey. *IEEE transactions on intelligent transportation systems*, 23(6): 4909–4926.
- Kong, Z.; Guo, J.; Li, A.; and Liu, C. 2020. Physgan: Generating physical-world-resilient adversarial examples for autonomous driving. In *Proceedings of the IEEE/CVF conference on computer vision and pattern recognition*, 14254–14263.
- Li, D.; Ren, J.; Wang, Y.; Wen, X.; Li, P.; Xu, L.; Zhan, K.; Xia, Z.; Jia, P.; Lang, X.; et al. 2025a. Finetuning generative trajectory model with reinforcement learning from human feedback. *arXiv preprint arXiv:2503.10434*.
- Li, Y.; Fan, L.; He, J.; Wang, Y.; Chen, Y.; Zhang, Z.; and Tan, T. 2024a. Enhancing end-to-end autonomous driving with latent world model. *arXiv preprint arXiv:2406.08481*.
- Li, Y.; Tian, M.; Zhu, D.; Zhu, J.; Lin, Z.; Xiong, Z.; and Zhao, X. 2025b. Drive-R1: Bridging Reasoning and Planning in VLMs for Autonomous Driving with Reinforcement Learning. *arXiv preprint arXiv:2506.18234*.
- Li, Z.; Li, K.; Wang, S.; Lan, S.; Yu, Z.; Ji, Y.; Li, Z.; Zhu, Z.; Kautz, J.; Wu, Z.; et al. 2024b. Hydra-mdp: End-to-end multimodal planning with multi-target hydra-distillation. *arXiv preprint arXiv:2406.06978*.
- Li, Z.; Yao, W.; Wang, Z.; Sun, X.; Chen, J.; Chang, N.; Shen, M.; Wu, Z.; Lan, S.; and Alvarez, J. M. 2025c. Generalized Trajectory Scoring for End-to-end Multimodal Planning. *arXiv preprint arXiv:2506.06664*.
- Liao, B.; Chen, S.; Yin, H.; Jiang, B.; Wang, C.; Yan, S.; Zhang, X.; Li, X.; Zhang, Y.; Zhang, Q.; et al. 2025. Diffusiondrive: Truncated diffusion model for end-to-end autonomous driving. In *Proceedings of the Computer Vision and Pattern Recognition Conference*, 12037–12047.
- Marler, R. T.; and Arora, J. S. 2004. Survey of multi-objective optimization methods for engineering. *Structural and multidisciplinary optimization*, 26(6): 369–395.
- Ouyang, L.; Wu, J.; Jiang, X.; Almeida, D.; Wainwright, C.; Mishkin, P.; Zhang, C.; Agarwal, S.; Slama, K.; Ray, A.; et al. 2022. Training language models to follow instructions with human feedback. *Advances in neural information processing systems*, 35: 27730–27744.
- Qian, K.; Jiang, S.; Zhong, Y.; Luo, Z.; Huang, Z.; Zhu, T.; Jiang, K.; Yang, M.; Fu, Z.; Miao, J.; et al. 2025a. Agentthink: A unified framework for tool-augmented chain-of-thought reasoning in vision-language models for autonomous driving. *arXiv preprint arXiv:2505.15298*.
- Qian, K.; Luo, Z.; Jiang, S.; Huang, Z.; Miao, J.; Ma, Z.; Zhu, T.; Li, J.; He, Y.; Fu, Z.; et al. 2025b. Fasionad++: Integrating high-level instruction and information bottleneck in fat-slow fusion systems for enhanced safety in autonomous driving with adaptive feedback. *arXiv preprint arXiv:2503.08162*.
- Qian, K.; Ma, Z.; He, Y.; Luo, Z.; Shi, T.; Zhu, T.; Li, J.; Wang, J.; Chen, Z.; He, X.; et al. 2024a. Fasionad: Fast and slow fusion thinking systems for human-like autonomous driving with adaptive feedback. *arXiv preprint arXiv:2411.18013*.
- Qian, K.; Miao, J.; Jiao, X.; Luo, Z.; Fu, Z.; Shi, Y.; Wang, Y.; Jiang, K.; and Yang, D. 2024b. Priormotion: Generative class-agnostic motion prediction with raster-vector motion field priors. *arXiv preprint arXiv:2412.04020*.
- Qian, K.; Miao, J.; Luo, Z.; Fu, Z.; Shi, Y.; Wang, Y.; Jiang, K.; Yang, M.; Yang, D.; et al. 2025c. LEGO-Motion: Learning-Enhanced Grids with Occupancy Instance Modeling for Class-Agnostic Motion Prediction. *arXiv preprint arXiv:2503.07367*.
- Qian, Z.; Jiang, K.; Cao, Z.; Qian, K.; Xu, Y.; Zhou, W.; and Yang, D. 2024c. SPIDER: Self-Driving Planners and Intelligent Decision-Making Engines with Reusability. In *2024*

- IEEE 27th International Conference on Intelligent Transportation Systems (ITSC)*, 937–944. IEEE.
- Rafailov, R.; Sharma, A.; Mitchell, E.; Manning, C. D.; Ermon, S.; and Finn, C. 2023. Direct preference optimization: Your language model is secretly a reward model. *Advances in neural information processing systems*, 36: 53728–53741.
- Shani, L.; Rosenberg, A.; Cassel, A.; Lang, O.; Calandriello, D.; Zipori, A.; Noga, H.; Keller, O.; Piot, B.; Szpektor, I.; et al. 2024. Multi-turn reinforcement learning with preference human feedback. *Advances in Neural Information Processing Systems*, 37: 118953–118993.
- Shao, H.; Wang, L.; Chen, R.; Li, H.; and Liu, Y. 2023. Safety-enhanced autonomous driving using interpretable sensor fusion transformer. In *Conference on Robot Learning*, 726–737. PMLR.
- Shao, Z.; Wang, P.; Zhu, Q.; Xu, R.; Song, J.; Bi, X.; Zhang, H.; Zhang, M.; Li, Y.; Wu, Y.; et al. 2024. Deepseekmath: Pushing the limits of mathematical reasoning in open language models. *arXiv preprint arXiv:2402.03300*.
- Shi, Y.; Jiang, K.; Wang, K.; Li, J.; Wang, Y.; Yang, M.; and Yang, D. 2024. Streamingflow: Streaming occupancy forecasting with asynchronous multi-modal data streams via neural ordinary differential equation. In *Proceedings of the IEEE/CVF Conference on Computer Vision and Pattern Recognition*, 14833–14842.
- Song, Z.; Liu, L.; Pan, H.; Liao, B.; Guo, M.; Yang, L.; Zhang, Y.; Xu, S.; Jia, C.; and Luo, Y. 2025. Breaking Imitation Bottlenecks: Reinforced Diffusion Powers Diverse Trajectory Generation. *arXiv preprint arXiv:2507.04049*.
- Sun, W.; Lin, X.; Shi, Y.; Zhang, C.; Wu, H.; and Zheng, S. 2024. Sparsedrive: End-to-end autonomous driving via sparse scene representation. *arXiv preprint arXiv:2405.19620*.
- Tang, X.; Kan, M.; Shan, S.; and Chen, X. 2025. Plan-R1: Safe and Feasible Trajectory Planning as Language Modeling. *arXiv preprint arXiv:2505.17659*.
- Wang, Y.; Pan, H.; Zhu, J.; Wu, Y.-H.; Zhan, X.; Jiang, K.; and Yang, D. 2022. Be-sti: Spatial-temporal integrated network for class-agnostic motion prediction with bidirectional enhancement. In *Proceedings of the IEEE/CVF Conference on Computer Vision and Pattern Recognition*, 17093–17102.
- Weng, X.; Ivanovic, B.; Wang, Y.; Wang, Y.; and Pavone, M. 2024. Para-drive: Parallelized architecture for real-time autonomous driving. In *Proceedings of the IEEE/CVF Conference on Computer Vision and Pattern Recognition*, 15449–15458.
- Wu, P.; Jia, X.; Chen, L.; Yan, J.; Li, H.; and Qiao, Y. 2022. Trajectory-guided Control Prediction for End-to-end Autonomous Driving: A Simple yet Strong Baseline. In *NeurIPS*.
- Xing, Z.; Zhang, X.; Hu, Y.; Jiang, B.; He, T.; Zhang, Q.; Long, X.; and Yin, W. 2025. Goalflow: Goal-driven flow matching for multimodal trajectories generation in end-to-end autonomous driving. In *Proceedings of the Computer Vision and Pattern Recognition Conference*, 1602–1611.
- Yang, Y.; Li, Y.; and Quan, X. 2021. Ubar: Towards fully end-to-end task-oriented dialog system with gpt-2. In *Proceedings of the AAAI conference on artificial intelligence*, volume 35, 14230–14238.
- Yang, Z.; Chai, Y.; Anguelov, D.; Zhou, Y.; Sun, P.; Erhan, D.; Rafferty, S.; and Kretschmar, H. 2020. Surfelgan: Synthesizing realistic sensor data for autonomous driving. In *Proceedings of the IEEE/CVF Conference on Computer Vision and Pattern Recognition*, 11118–11127.
- Yao, W.; Li, Z.; Lan, S.; Wang, Z.; Sun, X.; Alvarez, J. M.; and Wu, Z. 2025. DriveSuprim: Towards Precise Trajectory Selection for End-to-End Planning. *arXiv preprint arXiv:2506.06659*.
- Yu, W.; Peng, J.; Yang, H.; Zhang, J.; Duan, Y.; Ji, J.; and Zhang, Y. 2024. Ldp: A local diffusion planner for efficient robot navigation and collision avoidance. In *2024 IEEE/RSJ International Conference on Intelligent Robots and Systems (IROS)*, 5466–5472. IEEE.
- Yuan, C.; Zhang, Z.; Sun, J.; Sun, S.; Huang, Z.; Lee, C. D. W.; Li, D.; Han, Y.; Wong, A.; Tee, K. P.; et al. 2024. Drama: An efficient end-to-end motion planner for autonomous driving with mamba. *arXiv preprint arXiv:2408.03601*.
- Zadeh, L. 1963. Optimality and non-scalar-valued performance criteria. *IEEE transactions on Automatic Control*, 8(1): 59–60.
- Zhai, J.-T.; Feng, Z.; Du, J.; Mao, Y.; Liu, J.-J.; Tan, Z.; Zhang, Y.; Ye, X.; and Wang, J. 2023. Rethinking the Open-Loop Evaluation of End-to-End Autonomous Driving in nuScenes. *arXiv preprint arXiv:2305.10430*.
- Zhang, Y.; Qian, D.; Li, D.; Pan, Y.; Chen, Y.; Liang, Z.; Zhang, S.; Zhang, S.; Li, H.; Fu, M.; et al. 2024. Graphad: Interaction scene graph for end-to-end autonomous driving. *arXiv preprint arXiv:2403.19098*.
- Zheng, W.; Song, R.; Guo, X.; Zhang, C.; and Chen, L. 2024. Genad: Generative end-to-end autonomous driving. In *European Conference on Computer Vision*, 87–104. Springer.
- Zhou, J.; Lyu, L.; Tian, Z.; Zhuo, C.; and Li, Y. 2025. SafeMVDriVe: Multi-view Safety-Critical Driving Video Synthesis in the Real World Domain. *arXiv preprint arXiv:2505.17727*.
- Zhu, J.-Y.; Park, T.; Isola, P.; and Efros, A. A. 2017. Unpaired image-to-image translation using cycle-consistent adversarial networks. In *Proceedings of the IEEE international conference on computer vision*, 2223–2232.